

Local thermometry of NbSe₂ flake with delta- T noise measurements

M.G. Prokudina,¹ A.F. Shevchun,¹ and E.S. Tikhonov^{1,*}

¹*Osipyan Institute of Solid State Physics RAS, 142432 Chernogolovka, Russian Federation*

We perform transport and noise measurements for device consisting of a thin NbSe₂ flake laid onto the predefined gold electrodes and covered with a thin hBN flake. In the shot noise of a NbSe₂/Au tunnel junction (TJ), we identify Andreev reflection regime by demonstrating the effective charge doubling. Further, by creating temperature gradient across the TJ and measuring its delta- T noise in the normal state, we extract electron-phonon scattering length in NbSe₂ and its T -dependence. The results of delta- T noise measurements in the absence of a magnetic field when the flake is superconducting are in qualitative agreement with expectations. The introduced approach is promising for the study of nonequilibrium configurations in superconductors.

I. INTRODUCTION

Understanding of quasiparticle dynamics in superconductors is essential for improving the operation of superconductor based electronic microrefrigerators [1], photon detectors [2, 3], kinetic inductance elements [4] and qubits [5]. In a static measurement, one of the convenient approaches to the study of relaxation utilizes lithographically defined tunnel junctions (TJs) which can either provide local details of the electronic states via conductance tunnel spectroscopy [6], or may serve as a local injector of high-energy quasiparticles [7]. The most advanced methods exploit cryogenic scanning microscope techniques rather than lithographic TJs [8].

In the present manuscript, we implement the approach for local thermometry of electronic states in a nonequilibrium superconductor based on the noise measurements of a weakly coupled tunnel probe which serves as an energy preserving sensor [9]. Previously, similar approach was used for local thermometry of electronic states in diffusive metallic conductors using as a sensor InAs nanowires with negligible electron-phonon scattering [10], and consequently for energy resolution of electronic states in diffusive metallic wires with sensor represented by a TJ [11]. However, up to now this approach has never been applied to superconductors. We note that this approach doesn't rely on any spectral features of superconductor or the sensor so that its applicability is not limited by high temperatures or magnetic fields (B) like in tunnel conductance spectroscopy experiments [12].

Recently, along with conventional bulk superconducting materials, transition-metal dichalcogenides (TMDC) superconductors have also achieved much attention due to the high potential in nanoelectronics and nanophotonics applications [13]. TMDC layered materials offer an accessible platform with the possibility to go down to the few nanometers thickness range, assembling the devices using the now widespread stacking technique. One of the most extensively studied superconducting materials from the TMDC family is niobium diselenide. We introduce our local thermometry approach using as a

testbed the thin NbSe₂ flake which allows us to extract the electron-phonon coupling and the temperature (T) dependence of electron-phonon scattering length. Our findings are relevant for the possible nonequilibrium applications of NbSe₂ [14]. This approach can be used for the characterization of not only the other members of TMDC superconductors down to the 2D limit but also for the characterization of the bulk superconductors.

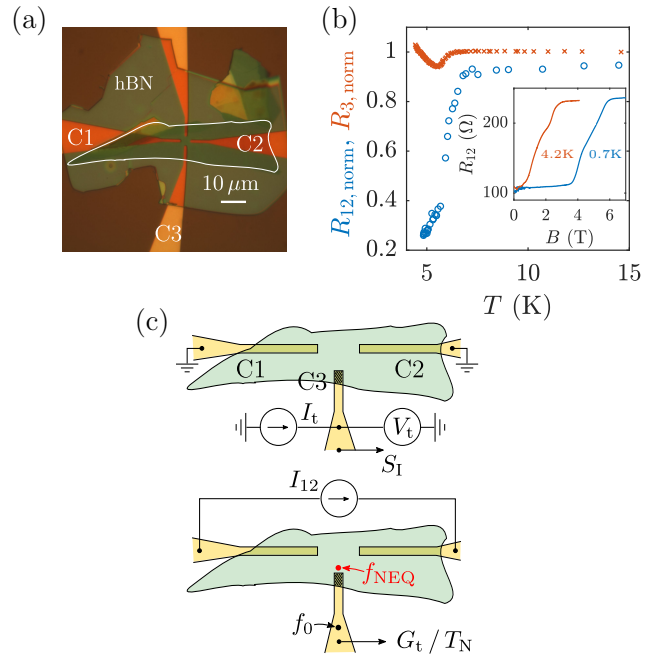


FIG. 1. (a) Optical micrograph of the device. Exfoliated NbSe₂ flake (marked with white line) is put on pre-patterned gold contacts and is then covered with hBN flake. Working contacts are marked with C1, C2 and C3. (b) Temperature dependence of the normalized resistances R_{12} (blue circles) and R_3 (red crosses). The inset demonstrates magnetic field dependence of R_{12} at $T = 4.2$ K (red) and 0.7 K (blue). (c) Measurement scheme for characterization of the tunnel junction realized at C3/NbSe₂ interface (up) and for conductance/noise spectroscopy (down).

* e-mail:tikhonov@issp.ac.ru

II. DEVICE FABRICATION AND ITS T - AND B -BEHAVIOR

Thin NbSe₂ flake is first mechanically exfoliated from commercial bulk crystal (HQgraphene) onto polydimethylsiloxane stamp and is then transferred to the prepatterned 30nm thick gold contacts on an oxidized silicon chip. The same procedure is then repeated for the hBN flake which is deposited above the NbSe₂ flake to protect it from oxidization. The optical micrograph of the device is shown in Fig. 1(a). All the measurements are performed in a ³He refrigerator at bath temperatures 4.2 K (gas) and 0.7 K (liquid). The magnetic field is perpendicular to the plane of the flake. The details of our noise measurements can be found in Supplemental Material of [15].

Out of four gold contact pads, three provide electrical contact to the flake (labelled with C1, C2 and C3). Fig. 1(b) demonstrates temperature (T) dependence of the normalized quasi- four-terminal linear-response resistances: R_{12} measured between pads C1 and C2 (blue circles), and R_3 measured between pads C3 and both pads C1 and C2 in parallel (red crosses). At room temperature these resistances are approximately 800 Ω and 6 k Ω , respectively. Upon cooling, in the vicinity of $T \approx 6$ K where the flake enters the superconducting transition region [16], both R_{12} and R_3 first demonstrate steep decrease. At further cooling, however, the behavior of $R_{12}(T)$ and $R_3(T)$ is different. While $R_{12}(T)$ monotonically decreases down to the lowest available $T = 0.7$ K, $R_3(T)$ starts increasing at around $T \approx 5$ K, reaching 6 k Ω at 4.2 K and 17 k Ω at 0.7 K (the T -dependence below 4.2 K is not shown). As we argue below, this behavior reflects the formation of a tunnel-type contact between the flake and the gold pad C3. Magnetic field destroys superconductivity of the flake, see the inset of Fig. 1(b) for the curves of $R_{12}(B)$ at both $T = 4.2$ K and 0.7 K. Additional transport data obtained on another exfoliated thin flake on prepatterned gold contacts as well as data obtained on lithographically patterned thick flake are demonstrated in Supplementary Material Fig. S1 and Fig. S2, respectively. We note that generally most of our interfaces between prepatterned gold and NbSe₂ turn out to be in the few hundred Ohms range and demonstrate monotonically decreasing $R(T)$ upon cooling down. The fact that some of the contacts demonstrate tunnel characteristics is occasional and is not controlled [17]. In Supplementary Material Fig. S3 we show one more example of a tunnel contact on another thin NbSe₂ flake.

III. TUNNEL JUNCTION CHARACTERIZATION

Using the schematics from the upper part of Fig. 1(c), we now characterize transport and noise properties of the TJ. Here, we can safely neglect the contribution to the measured resistance from both interfaces

C1(C2)/NbSe₂ and from the flake itself since these resistances are limited by no more than approximately 100 Ω , see the inset of Fig. 1(b). In high enough magnetic fields, TJ's I - V characteristics is linear at both $T = 4.2$ K and 0.7 K so that the differential conductance, $G_t = dI_t/dV_t$, is bias-independent, see red circles in Fig. 2(a) for the normalized to high bias voltage data at $T = 0.7$ K in the magnetic field $B = 5.1$ T. Upon decreasing B , $G_t(V_t)$ starts demonstrating features inherent to NS-contacts in the tunnelling regime. Namely, we observe the peaks in $G_t(V_t)$ curves which are most pronounced in $B = 0$ (blue circles). Moreover, these peaks smooth out upon increasing temperature (yellow circles).

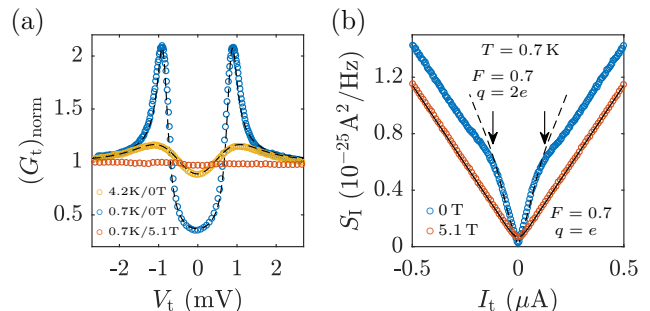


FIG. 2. (a) Normalized differential conductance of the tunnel probe. The dashed lines are fits according to the BTK model using $\Delta = 0.69$ meV, $Z = 1.03$ at 4.2 K and $\Delta = 0.88$ meV, $Z = 1.12$ at 0.7 K. (b) Current noise spectral density of the tunnel probe at $T = 0.7$ K in a magnetic field of $B = 0$ and 5.1 T. Dashed lines are the fits with $F = 0.7$ and $q = e$ in $B = 5.1$ T and $q = 2e$ in $B = 0$ T (see text).

Quantitative description of differential conductance curves of NS-contacts is usually performed by comparison to the behavior predicted by the BTK-model [18],

$$I_{\text{NS}} \propto \int_{-\infty}^{+\infty} [f_0(\varepsilon - eV) - f_0(\varepsilon)] [1 + A(\varepsilon) - B(\varepsilon)],$$

where $A(\varepsilon)$ and $B(\varepsilon)$ are the Andreev and normal reflection probabilities listed in Table II of ref. [18] and depending on the dimensionless number Z which specifies the strength of the interface potential barrier. We observe that the above expression provides reasonable agreement with the experimental data, see the dashed lines in Fig. 2(a). The used fitting parameters are $\Delta = 0.69$ meV, $Z = 1.03$ at 4.2 K and $\Delta = 0.88$ meV, $Z = 1.12$ at 0.7 K. We note that such obtained Z is almost T -independent, and the values of superconducting gap potential Δ at two temperatures fall on the expected T -dependence of superconducting gap, $\Delta \propto \tanh\left(1.74\sqrt{T_c/T - 1}\right)$, with the superconducting transition temperature $T_c = 5.9$ K. Overall, the data of Fig. 2(a) indicate that the C3/NbSe₂ interface is represented by a TJ which is characterized by the set of

energy-independent transmission probabilities which on the average may be estimated as $\langle\tau\rangle\sim(1+Z^2)^{-1}\approx 0.5$. From here, we expect the number of spin-degenerate conduction channels across the C3/NbSe₂ interface as $N = h/(2e^2\langle\tau\rangle R_N) \approx 5$, where $R_N \approx 5\text{ k}\Omega$ is the normal state low-temperature resistance. The obtained result corresponds, most likely, to a point contact with the cross-section area being on the order of 1 nm^2 .

Additional information is provided by the standard noise measurements [19]. Here, we pass the current I_t across the TJ like in differential conductance measurements, see the upper part of Fig. 1(c), and measure the voltage fluctuations utilizing the resonant tank circuit technique with the central frequency of approximately 15 MHz. The results expressed in terms of the current noise spectral density, S_I , as a function of I_t , are demonstrated in Fig. 2(b). At $T = 0.7\text{ K}$, in high enough magnetic field $B = 5.1\text{ T}$ where the TJ's I - V characteristics is linear (red circles), we observe linear growth of S_I with the absolute value of I_t . In the whole range of TJ currents, the data are perfectly consistent (see the solid black line) with the standard shot noise expression

$$S_I = 4k_B T G + 2q|I|F(\coth\xi - 1/\xi), \quad (1)$$

where $G = G_t$ is the TJ differential conductance, $I = I_t$ is the current through the TJ, $q = e$ is the electron charge, $\xi = q|V|/(2k_B T)$ is determined by the TJ bias voltage $V = V_t$, and $F = 0.7$. Note that for the single-channel TJ, based on the estimate from the BTK fits for the differential conductance one should have expected $F = 1 - \tau \approx 0.5$. Important for further discussion is the linear dependence of $S_I(I_t)$ revealing the lack of electron-phonon relaxation in transport across the TJ.

In zero magnetic field, the $S_I(I_t)$ -curve (blue circles) demonstrates two kinks at currents corresponding to the bias voltages $(V_t)_{\text{kink}} \approx \pm\Delta/e = 0.88\text{ mV}$, see arrows in Fig. 2(b). Quantitatively, the low current data are reasonably described using the same expression (1) but now with $q = 2e$, while the slope of the high current data is the same as for the case of $B = 5.1\text{ T}$. This behavior is expected [20] and reflects the Andreev reflection mechanism in transport across NS contacts [21–25]: at sub-gap voltages the current is converted directly into supercurrent which is accomplished by the reflection of a hole back into the metal so that charge $2e$ is transferred across the interface.

IV. GOOD CONTACTS CHARACTERIZATION

Unlike C3/NbSe₂ interface, both interfaces C1(C2)/NbSe₂ are relatively transparent. In Fig. 3(a) we plot B -evolution of the differential resistance dV_{12}/dI_{12} at low biases, measured at $T = 0.7\text{ K}$. The blue curve, corresponding to $B = 0$, exhibits a set of resistance peaks. These peaks are absent at $T = 4.2\text{ K}$ (see Supplementary Material Fig. S4) and smooth out at increasing B . We note that single peaks at

few mV bias voltages similar to our biggest peaks were also observed in [26] at intermediate $T = 3.3\text{ K}$. As we demonstrate below, even at the lowest available $T = 0.7\text{ K}$ electron-phonon scattering length $l_{e\text{-ph}}$ in NbSe₂ is much shorter than the distance between two interfaces so that the device should be considered as a series connection of two independent NS interfaces and the flake itself. In our device it is not possible to reliably separate contribution of two interfaces to R_{12} . We note that for the single graphene/NbSe₂ interface, the recent paper [27] identified similar peaks as originating from the transport between the superconductor and the proximitized conductor underneath, in our case corresponding to the transport across the proximitized Au/NbSe₂ interface. The occurrence of multiple peaks may be related to the varying NbSe₂ thickness along the interface. The corresponding evolution of differential resistance R_{12} with magnetic field and bias voltage is demonstrated in Supplementary Material Fig. S5.

Similar to the findings of [27], we also observe the voltage steps in the current-voltage characteristics $V_{12}(I_{12})$, at large bias currents around 0.4 mA . The corresponding zero-field data are demonstrated in Fig. 3(b) by blue and red curves corresponding to the opposite current sweep directions. These steps get smoothed out at relatively small magnetic fields as shown by three more curves in Fig. 3(b). Overall, the observed hysteresis along with the B -behavior indicate the superconducting origin of the steps. Qualitatively similar hysteretic behavior was recently reported for the geometrically well-defined system represented by a semiconducting full-shell epitaxial Al-InAs nanowire connected on its ends to two thick Au pads [28]. It was demonstrated that observation of superconducting state at bias voltages $V \gg \Delta/e$ implies strong energy relaxation. Compared to the one-dimensional wire-shaped geometry of [28], in our case poorly defined two-dimensional geometry for current redistribution results in multiple hysteretic steps in the I - V characteristics rather than to a single hysteretic loop. Yet another important difference is the stronger electron-phonon relaxation in NbSe₂ compared to Al (see below), leading to observation of superconducting state even further above the superconducting gap.

V. CONDUCTANCE SPECTROSCOPY

Evolution of local superconducting state in the flake in the presence of bias current can be visualized by the widely accepted conductance tunnel probe spectroscopy [8, 18, 29–33] using the TJ at the C3/NbSe₂ interface, see the bottom part of Fig. 1(c). Fig. 3(c) demonstrates the color-scale plot of the differential conductance of the tunnel probe G_t as a function of the tunnel probe bias voltage V_t and of the current through the flake I_{12} , measured at $T = 4.2\text{ K}$ with the sweep of I_{12} from positive to negative values. We were not able to perform similar measurements at 0.7 K since at low T the

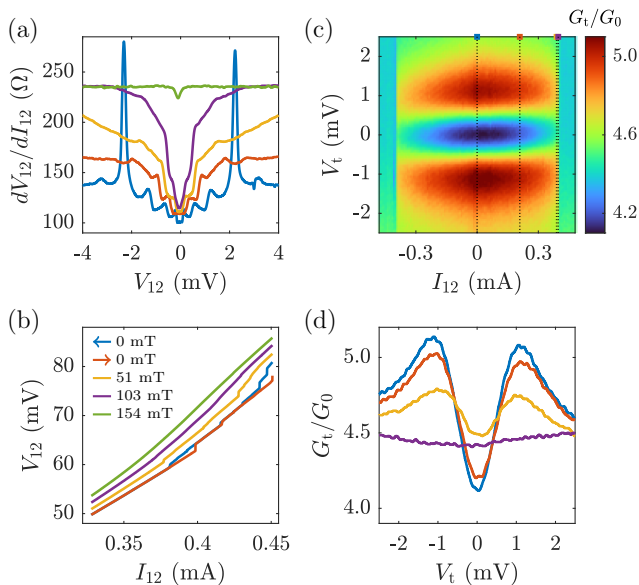


FIG. 3. (a) Differential resistance of the flake as a function of bias voltage in magnetic fields of $B = 0, 2.1, 3.1, 4.1$ and 5.7 T (from blue to green curves). (b) I - V curve of the flake demonstrating the voltage steps and their evolution in a magnetic field at $T = 4.2$ K. (c) Differential conductance of the tunnel probe as a function of flake current I_{12} and the tunnel probe bias voltage at $T = 4.2$ K. (d) Linecuts of differential conductance at specific values of $I_{\text{flake}} = 0, 0.21, 0.389$ and 0.397 mA indicated by dashed lines on panel (c).

device was generating some noise overloading the preamplifier at large values of $|I_{12}|$. The shaded squares with the corresponding dashed black lines in Fig. 3(c) indicate the specific values of I_{12} for which $G_t(V_t)$ are shown in Fig. 3(d). Below the transition value of $I_{12} \approx 0.39$ mA, at decreasing the magnitude of I_{12} , the tunnel probe differential conductance gradually evolves in a way so that conductance peaks move to larger values of $|V_t|$ and the zero-bias conductance dip becomes more pronounced. This indicates the continuous decrease of the local electronic temperature T_e in the vicinity of the TJ. The result of Fig. 3(c) allows us to demonstrate the qualitative difference of our case compared to the situation where one can neglect electronic energy relaxation. Namely, we note that the transition between local superconducting and normal states happens in a similar way regardless of whether $|I_{12}|$ decreases or increases. In contrast, for the Al wire shorter than electron-phonon scattering length and connected between two large copper pads [31], evolution of superconducting state was shown to differ depending on the current sweep direction. The difference comes from the realization in the case of negligible energy relaxation [31] of the so-called global and bimodal superconducting states for two opposite current sweep directions. The global state is one coherent superconducting state extending over the full length of the wire and realized for the increasing current sweep, while the bimodal

state consists of two separate superconducting domains located at each cold end of the wire and realized for the decreasing current sweep. Strong energy relaxation in NbSe₂ makes this picture inapplicable in our case.

VI. DELTA- T NOISE MEASUREMENTS

One way to experimentally quantify electron-phonon relaxation in a device is to measure its current noise [34–37]. Namely, for the two-terminal diffusive conductor without electron-phonon scattering its shot noise is described by (1) with $F = 1/3$ and $F = \sqrt{3}/4$ for the cases of negligible and strong electron-electron scattering, respectively. For the diffusive conductor, suppression of the current noise below $F = 1/3$ indicates the relevance of electron-phonon scattering which is characterized by electron-phonon coupling $\Sigma_{e\text{-ph}}$ entering to the power flow from electron to phonon subsystem via

$$P_{e\text{-ph}} = \mathcal{V} \Sigma_{e\text{-ph}} (T_e^n - T_{\text{ph}}^n), \quad (2)$$

where \mathcal{V} is the system volume, T_e and T_{ph} are electronic and phononic temperatures, and exponent n typically varies in the range $n \approx 3 - 5$ [1]. In the steady state $P_{e\text{-ph}}$ is exactly the released Joule heat power. The relation (2) works best for the case of long enough devices where T_e and T_{ph} can be considered as position-independent everywhere besides short regions near the terminals. From the experimental point of view, special care should be paid to ensure that contact pads and the corresponding interfaces do not contribute to the measured noise signal [38]. If the device under study is a superconductor connected to normal contacts, taking contacts into account turns out to be a fundamental difficulty which can not be overcome in standard noise thermometry. In the present case of a thin NbSe₂ flake which degrades during the standard lithography techniques, the proper quality of contacts can hardly be ensured for the thermometry experiment even on the flake in the normal state.

Below we will perform a local delta- T noise experiment which is advantageous [10, 11, 39] in this situation, see the schematics from the bottom part of Fig. 1(c). Consider a TJ characterized by energy-independent transmission probabilities τ_n and differential conductance G_t , which connects two conductors: the one in equilibrium with Fermi-Dirac energy distribution (ED), $f_0(\varepsilon, T_0) = [\exp(\varepsilon/k_B T_0) + 1]^{-1}$, and the nonequilibrium one with some ED $f_{\text{NEQ}}(\varepsilon)$ which is generally position-dependent. Here T_0 is the bath temperature and the two conductors in our case are represented by the gold pad C3 and the NbSe₂ flake, respectively, see the lower part of Fig. 1(c) with the shaded region representing the TJ. Generally, the noise temperature of a TJ under applied bias voltage V_t , $T_N(V_t) = S_I/4k_B G_t$, allows one to extract [9, 11, 40]

$$f_{\text{NEQ}}(\varepsilon) = \frac{1}{2} - \frac{1}{F} \frac{d(k_B T_N)}{d(eV_t)} \Big|_{eV_t = \varepsilon}. \quad (3)$$

Here $S_I(V_t)$ is the TJ's current noise spectral density, $F = \sum \tau_n(1 - \tau_n) / \sum \tau_n$ is the Fano-factor of the TJ and V_t is the bias voltage on it. This relation is valid provided T_0 is much smaller than the characteristic energy scale on which $f_{\text{NEQ}}(\varepsilon)$ changes significantly.

The important special case is realized for nonequilibrium conductors with strong electron-electron or electron-phonon relaxation so that $f_{\text{NEQ}}(\varepsilon)$ is of Fermi-Dirac type, $f_{\text{NEQ}}(\varepsilon) = f_0(\varepsilon, T_e) \equiv [\exp(\varepsilon/k_B T_e) + 1]^{-1}$, with nonequilibrium electronic temperature T_e . In this particular case, the local value of T_e can be extracted from the noise measurements using [19]

$$T_N = \frac{T_e + T_0}{2} + \frac{F}{2k_B} \int d\varepsilon [f_0(\varepsilon, T_e) - f_0(\varepsilon, T_0)]^2, \quad (4)$$

applicable, in contrast to (3), at any value of T_e . Note there is no average current through the TJ and the nonequilibrium noise comes from different temperatures on two sides of the TJ. Below we will use (4) to obtain the local value of T_e in the vicinity of the TJ in the driven out-of-equilibrium NbSe₂ flake from the measurements of T_N . Note that this relation assumes the condition $G_t \ll R_{12}^{-1}$ which assures the negligible heat conduction across the TJ.

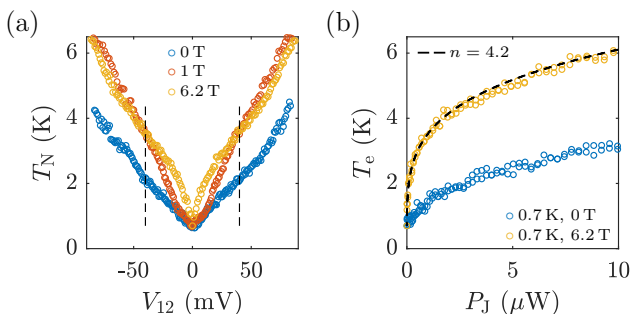


FIG. 4. (a) Noise temperature of the TJ as a function of bias voltage on the flake in $B = 0, 1$ and 6.2 T measured at bath temperature $T_0 = 0.7$ K. Dashed lines indicate the range of bias voltages used for the analysis in panel (b). (b) Local electronic temperature in NbSe₂ under the TJ as a function of the total Joule power released in the flake due to the current I_{12} . Dashed line is a fit using (2) with $n = 4.2$ and $\mathcal{V}_{\Sigma_{\text{e-ph}}} = 5 \cdot 10^{-9} \text{ W/K}^{4.2}$.

In the experiment we measure voltage fluctuations of a TJ in response to the bias current through the flake. We concentrate on the low- T data obtained at $T = 0.7$ K where the exponent n entering (2) can be extracted unambiguously due to the relatively large range of accessible T_N . The data expressed in terms of noise temperature T_N of a TJ as a function of bias voltage V_{12} on the flake are demonstrated in Fig. 4(a) for the three representative values of magnetic field. The main effect of B on the $T_N(V_{12})$ curves occurs in the bias range below approximately 40 mV (see the vertical dashed lines) where the slope of the curves grows significantly with the increasing

magnetic field. Further, we limit ourselves to this region of $|V_{12}| \lesssim 40$ mV where the dependencies $T_N(V_{12})$ are sublinear. As is evident from Fig. 4(a), at larger bias voltages these dependencies tend to linear ones which may indicate mediated by amorphous SiO₂ relaxation bottleneck with $n \approx 2$ [41, 42].

Using (4), from the data of Fig. 4(a) we extract the local electronic temperature in the NbSe₂ flake in the vicinity of the TJ. The results are demonstrated in Fig. 4(b). In $B = 6.2$ T the flake is in the normal state, see the inset of Fig. 1(b), and the power flow between electron and phonon subsystems is well described by (2) with $T_0 = 0.7$ K, $n = 4.2$ and $\mathcal{V}_{\Sigma_{\text{e-ph}}} = 5 \cdot 10^{-9} \text{ W/K}^{4.2}$, see yellow symbols and the corresponding black dashed fit in Fig. 4(b). This value allows one to estimate the electron-phonon scattering length in NbSe₂ via [43]

$$l_{\text{e-ph}} = L [\mathcal{L}/nT^{n-2}\mathcal{V}_{\Sigma_{\text{e-ph}}}R_{12}]^{1/2},$$

where L is the effective device length and $\mathcal{L} = 2.44 \cdot 10^{-8} \text{ W}\Omega\text{K}^{-2}$ is the Lorenz number. Importantly, even at the lowest available $T_0 = 0.7$ K, $l_{\text{e-ph}}$ is approximately 10 times shorter than the effective device length, $l_{\text{e-ph}}/L \approx 0.1$, demonstrating the importance of energy relaxation in any nonequilibrium experiment with NbSe₂ on a micrometer scale. Quantitatively, the effective device length in our case can be roughly estimated on the order of 10 μm implying $l_{\text{e-ph}} \approx 0.8 \mu\text{m}/(T[\text{K}])^{1.1}$. It justifies the assumption made about the Fermi-Dirac shape of ED in the flake region near the C3/NbSe₂ interface. Note that observation of $n \approx 4$ excludes diffusion of heat into metallic contact pads as a dominant relaxation mechanism in the considered energy range which would be manifested in the observation of $n = 2$ [44]. We also note that observation of $n \approx 4$ may reflect the 2D nature of acoustic phonons similar to the case of graphene [45–48].

The above analysis implies that Joule heat is predominantly released in the NbSe₂ flake itself. However, from the magnetoresistance data presented in the inset of Fig. 1(c) one can estimate that in the normal state the flake resistance is only 1.5 times greater than the total interfaces resistance. We therefore deduce that our result allows for the spread $\mathcal{V}_{\Sigma_{\text{e-ph}}} \approx (3-5) \cdot 10^{-9} \text{ W/K}^{4.2}$. From here, $l_{\text{e-ph}}$ may be approximately 30% greater than estimated above. Still, we emphasize that our result for electron-phonon relaxation length in NbSe₂ in the normal state, $l_{\text{e-ph}}(\text{NbSe}_2, 0.7 \text{ K}) \approx 1 \mu\text{m}$, is significantly smaller than the recent results [49] obtained for the normal state Al at the same T . Namely, acquired by the measurements of the dynamical response of thermal noise to an ac excitation, the values of D , A and n presented in Table I of ref. [49] suggest that $l_{\text{e-ph}}(\text{Al}, 0.7 \text{ K})$ lies in the range $3 \mu\text{m} - 9 \mu\text{m}$ for the relatively low-quality Al with the diffusion coefficient $D \lesssim 50 \text{ cm}^2/\text{s}$. Our results for the normal state NbSe₂ also suggest the weaker T -dependence of the electron-phonon scattering rate, $\tau_{\text{e-ph}}(\text{NbSe}_2) \propto T^{-2.2}$, compared to the clean metallic three-dimensional case where one would expect the $\propto T^{-3}$ -dependence.

In zero magnetic field, the NbSe₂ flake is superconducting so that Joule heat due to current I_{12} releases exclusively at C1(C2)/NbSe₂ interfaces. In this case, since the distance between interfaces and the tunnel probe is few times greater than electron-phonon scattering length, the increase of local electronic temperature nearby the probe at a given value of P_J may be expected to be smaller compared to the normal state case. This is indeed what we observe, see blue symbols in Fig. 4(b). In contrast to the normal case, temperature increase is now detected not where heat is released so that the role of heat conduction increases. Whether heat conduction in our device occurs by quasiparticle transport in NbSe₂ or by phonons in either of the 2D crystals NbSe₂ and hBN is not possible to conclude from our experiment and requires better defined geometry.

VII. CONCLUSIONS

In conclusion, we performed transport and noise measurements for a thin superconducting NbSe₂ flake laid

onto the predefined gold contacts and covered with a thin hBN flake. Tunnel junction formed at one of the NbSe₂/Au interfaces was utilized in two ways. First, by observation of effective charge doubling in the shot noise of this TJ at sub-gap energies, we identified Andreev reflection regime corresponding to tunneling across NS contact. Second, releasing Joule heat power on the NbSe₂ side of the TJ and measuring the resulting δT noise of the TJ, we extracted electron-phonon scattering length in NbSe₂ to be $l_{e-ph} \approx 0.8 \mu\text{m}/(T[\text{K}])^{1.1}$. Given the introduced approach is applied to geometrically well-defined superconducting devices, it is promising in the study of nonequilibrium configurations.

ACKNOWLEDGMENTS

We thank V.S. Khrapai and D.V. Shovkun for helpful discussions.

-
- [1] F. Giazotto, T. T. Heikkilä, A. Luukanen, A. M. Savin, and J. P. Pekola, Opportunities for mesoscopies in thermometry and refrigeration: Physics and applications, *Reviews of Modern Physics* **78**, 217 (2006).
 - [2] G. N. Gol'tsman, O. Okunev, G. Chulkova, A. Lipatov, A. Semenov, K. Smirnov, B. Voronov, A. Dzardanov, C. Williams, and R. Sobolewski, Picosecond superconducting single-photon optical detector, *Applied Physics Letters* **79**, 705 (2001).
 - [3] E. D. Walsh, W. Jung, G.-H. Lee, D. K. Efetov, B.-I. Wu, K.-F. Huang, T. A. Ohki, T. Taniguchi, K. Watanabe, P. Kim, D. Englund, and K. C. Fong, Josephson junction infrared single-photon detector, *Science* **372**, 409 (2021).
 - [4] L. Grünhaupt, N. Maleeva, S. T. Skacel, M. Calvo, F. Levy-Bertrand, A. V. Ustinov, H. Rotzinger, A. Monfardini, G. Catelani, and I. M. Pop, Loss Mechanisms and Quasiparticle Dynamics in Superconducting Microwave Resonators Made of Thin-Film Granular Aluminum, *Physical Review Letters* **121**, 117001 (2018).
 - [5] K. Serniak, M. Hays, G. De Lange, S. Diamond, S. Shankar, L. D. Burkhardt, L. Frunzio, M. Houzet, and M. H. Devoret, Hot Nonequilibrium Quasiparticles in Transmon Qubits, *Physical Review Letters* **121**, 157701 (2018).
 - [6] L. D. Alegria, C. G. L. Böttcher, A. K. Saydjari, A. T. Pierce, S. H. Lee, S. P. Harvey, U. Vool, and A. Yacoby, High-energy quasiparticle injection into mesoscopic superconductors, *Nature Nanotechnology* **16**, 404 (2021).
 - [7] S. B. Kaplan, J. R. Kirtley, and D. N. Langenberg, Experimental Determination of the Quasiparticle Energy Distribution in a Nonequilibrium Superconductor, *Physical Review Letters* **39**, 291 (1977).
 - [8] T. Jalabert, E. F. C. Driessen, F. Gustavo, J. L. Thomassin, F. Levy-Bertrand, and C. Chapelier, Thermalization and dynamics of high-energy quasiparticles in a superconducting nanowire, *Nature Physics* **19**, 956 (2023).
 - [9] T. Gramspacher and M. Büttiker, Local densities, distribution functions, and wave-function correlations for spatially resolved shot noise at nanocontacts, *Physical Review B* **60**, 2375 (1999).
 - [10] E. S. Tikhonov, D. V. Shovkun, D. Ercolani, F. Rossella, M. Rocci, L. Sorba, S. Roddaro, and V. S. Khrapai, Local noise in a diffusive conductor, *Scientific Reports* **6**, 30621 (2016).
 - [11] E. S. Tikhonov, A. O. Denisov, S. U. Piatrusha, I. N. Khrapach, J. P. Pekola, B. Karimi, R. N. Jabdaraghi, and V. S. Khrapai, Spatial and energy resolution of electronic states by shot noise, *Physical Review B* **102**, 085417 (2020).
 - [12] H. Pothier, S. Guéron, N. O. Birge, D. Esteve, and M. H. Devoret, Energy Distribution Function of Quasiparticles in Mesoscopic Wires, *Physical Review Letters* **79**, 3490 (1997).
 - [13] D. Qiu, C. Gong, S. Wang, M. Zhang, C. Yang, X. Wang, and J. Xiong, Recent Advances in 2D Superconductors, *Advanced Materials* **33**, 2006124 (2021).
 - [14] K. Shein, E. Zharkova, M. Kashchenko, A. Kolbatova, A. Lyubchak, L. Elesin, E. Nguyen, A. Semenov, I. Charaev, A. Schilling, G. Goltsman, K. S. Novoselov, I. Gayduchenko, and D. A. Bandurin, Fundamental Limits of Few-Layer NbSe₂ Microbolometers at Terahertz Frequencies, *Nano Letters* **24**, 2282 (2024).
 - [15] E. S. Tikhonov, M. Yu. Melnikov, D. V. Shovkun, L. Sorba, G. Biasiol, and V. S. Khrapai, Nonlinear transport and noise thermometry in quasiclassical ballistic point contacts, *Physical Review B* **90**, 161405 (2014).
 - [16] E. Khestanova, J. Birkbeck, M. Zhu, Y. Cao, G. L. Yu, D. Ghazaryan, J. Yin, H. Berger, L. Forró, T. Taniguchi, K. Watanabe, R. V. Gorbachev, A. Mishchenko, A. K.

- Geim, and I. V. Grigorieva, Unusual Suppression of the Superconducting Energy Gap and Critical Temperature in Atomically Thin NbSe₂, *Nano Letters* **18**, 2623 (2018).
- [17] N. Hoshi, D. Inoue, H. Sonoda, D. Yabe, H. Tomori, and A. Kanda, Response of a superconductor nbse2 flake to magnetic field detected with small tunnel junctions, *Journal of Physics: Conference Series* **1293**, 012016 (2019).
- [18] G. E. Blonder, M. Tinkham, and T. M. Klapwijk, Transition from metallic to tunneling regimes in superconducting microconstrictions: Excess current, charge imbalance, and supercurrent conversion, *Physical Review B* **25**, 4515 (1982).
- [19] Ya.M. Blanter and M. Büttiker, Shot noise in mesoscopic conductors, *Physics Reports* **336**, 1 (2000).
- [20] C. W. J. Beenakker, Random-Matrix Theory of Quantum Transport, *Reviews of Modern Physics* **69**, 731 (1997).
- [21] X. Jehl, M. Sanquer, R. Calemczuk, and D. Mailly, Detection of doubled shot noise in short normal-metal/ superconductor junctions, *Nature* **405**, 50 (2000).
- [22] A. A. Kozhevnikov, R. J. Schoelkopf, and D. E. Prober, Observation of Photon-Assisted Noise in a Diffusive Normal Metal–Superconductor Junction, *Physical Review Letters* **84**, 3398 (2000).
- [23] A. Das, Y. Ronen, M. Heiblum, D. Mahalu, A. V. Kretinin, and H. Shtrikman, High-efficiency Cooper pair splitting demonstrated by two-particle conductance resonance and positive noise cross-correlation, *Nature Communications* **3**, 1165 (2012).
- [24] Y. Ronen, Y. Cohen, J.-H. Kang, A. Haim, M.-T. Rieder, M. Heiblum, D. Mahalu, and H. Shtrikman, Charge of a quasiparticle in a superconductor, *Proceedings of the National Academy of Sciences* **113**, 1743 (2016).
- [25] A. Denisov, A. Bubis, S. Piatrusha, N. Titova, A. Nasibulin, J. Becker, J. Treu, D. Ruhstorfer, G. Koblmüller, E. Tikhonov, and V. Khrapai, Heat-Mode Excitation in a Proximity Superconductor, *Nanomaterials* **12**, 1461 (2022).
- [26] N. Paradiso, A.-T. Nguyen, K. Enzo Kloss, and C. Strunk, Phase slip lines in superconducting few-layer NbSe₂ crystals, *2D Materials* **6**, 025039 (2019).
- [27] R. Moriya, N. Yabuki, and T. Machida, Superconducting proximity effect in a NbSe₂/graphene van der Waals junction, *Physical Review B* **101**, 054503 (2020).
- [28] E. V. Shpagina, E. S. Tikhonov, D. Ruhstorfer, G. Koblmüller, and V. S. Khrapai, Fate of the superconducting state in floating islands of hybrid nanowire devices, *Phys. Rev. B* **109**, L140501 (2024).
- [29] A. Anthore, H. Pothier, and D. Esteve, Density of States in a Superconductor Carrying a Supercurrent, *Physical Review Letters* **90**, 127001 (2003).
- [30] H. Le Sueur, P. Joyez, H. Pothier, C. Urbina, and D. Esteve, Phase Controlled Superconducting Proximity Effect Probed by Tunneling Spectroscopy, *Physical Review Letters* **100**, 197002 (2008).
- [31] N. Vercruyssen, T. G. A. Verhagen, M. G. Flokstra, J. P. Pekola, and T. M. Klapwijk, Evanescent states and nonequilibrium in driven superconducting nanowires, *Physical Review B* **85**, 224503 (2012).
- [32] G. C. Ménard, S. Guissart, C. Brun, S. Pons, V. S. Stolyarov, F. Debontridder, M. V. Leclerc, E. Janod, L. Cario, D. Roditchev, P. Simon, and T. Cren, Coherent long-range magnetic bound states in a superconductor, *Nature Physics* **11**, 1013 (2015).
- [33] T. Dvir, F. Masee, L. Attias, M. Khodas, M. Aprili, C. H. L. Quay, and H. Steinberg, Spectroscopy of bulk and few-layer superconducting NbSe₂ with van der Waals tunnel junctions, *Nature Communications* **9**, 598 (2018).
- [34] M. L. Roukes, M. R. Freeman, R. S. Germain, R. C. Richardson, and M. B. Ketchen, Hot electrons and energy transport in metals at millikelvin temperatures, *Physical Review Letters* **55**, 422 (1985).
- [35] A. H. Steinbach, J. M. Martinis, and M. H. Devoret, Observation of Hot-Electron Shot Noise in a Metallic Resistor, *Physical Review Letters* **76**, 3806 (1996).
- [36] B. Huard, H. Pothier, D. Esteve, and K. E. Nagaev, Electron heating in metallic resistors at sub-Kelvin temperature, *Physical Review B* **76**, 165426 (2007).
- [37] A. C. Betz, S. H. Jhang, E. Pallecchi, R. Ferreira, G. Fève, J.-M. Berroir, and B. Plaçais, Supercollision cooling in undoped graphene, *Nature Physics* **9**, 109 (2013).
- [38] B. A. Polyak, V. S. Khrapai, and E. S. Tikhonov, What Can we Learn from Nonequilibrium Response of a Strange Metal?, *JETP Letters* **119**, 610 (2024).
- [39] O. S. Lumbroso, L. Simine, A. Nitzan, D. Segal, and O. Tal, Electronic noise due to temperature differences in atomic-scale junctions, *Nature* **562**, 240 (2018).
- [40] T. Ota, M. Hashisaka, K. Muraki, and T. Fujisawa, Negative and positive cross-correlations of current noises in quantum Hall edge channels at bulk filling factor $\nu = 1$, *Journal of Physics: Condensed Matter* **29**, 225302 (2017).
- [41] E. M. Baeva, N. A. Titova, A. I. Kardakova, S. U. Piatrusha, and V. S. Khrapai, Universal Bottleneck for Thermal Relaxation in Disordered Metallic Films, *JETP Letters* **111**, 104 (2020).
- [42] E. M. Baeva, N. A. Titova, L. Veyrat, B. Sacépé, A. V. Semenov, G. N. Goltsman, A. I. Kardakova, and Vadim. S. Khrapai, Thermal Relaxation in Metal Films Limited by Diffuson Lattice Excitations of Amorphous Substrates, *Physical Review Applied* **15**, 054014 (2021).
- [43] A. O. Denisov, E. S. Tikhonov, S. U. Piatrusha, I. N. Khrapach, F. Rossella, M. Rocci, L. Sorba, S. Roddaro, and V. S. Khrapai, Strategy for accurate thermal biasing at the nanoscale, *Nanotechnology* **31**, 324004 (2020).
- [44] M. Henny, S. Oberholzer, C. Strunk, and C. Schönberger, 1/3-shot-noise suppression in diffusive nanowires, *Phys. Rev. B* **59**, 2871 (1999).
- [45] S. S. Kubakaddi, Interaction of massless Dirac electrons with acoustic phonons in graphene at low temperatures, *Physical Review B* **79**, 075417 (2009).
- [46] A. M. R. Baker, J. A. Alexander-Webber, T. Altbauer, and R. J. Nicholas, Energy relaxation for hot Dirac fermions in graphene and breakdown of the quantum Hall effect, *Physical Review B* **85**, 115403 (2012).
- [47] A. C. Betz, F. Vialla, D. Brunel, C. Voisin, M. Picher, A. Cavanna, A. Madouri, G. Fève, J.-M. Berroir, B. Plaçais, and E. Pallecchi, Hot Electron Cooling by Acoustic Phonons in Graphene, *Physical Review Letters* **109**, 056805 (2012).
- [48] K. C. Fong and K. C. Schwab, Ultrasensitive and Wide-Bandwidth Thermal Measurements of Graphene at Low Temperatures, *Physical Review X* **2**, 031006 (2012).
- [49] E. Pinsolle, A. Rousseau, C. Lupien, and B. Reulet, Direct Measurement of the Electron Energy Relaxation Dynamics in Metallic Wires, *Physical Review Letters* **116**, 236601 (2016).

Supplementary Material to the article “Local thermometry of NbSe₂ flake with delta- T noise measurements”

I. ANOTHER THIN FLAKE

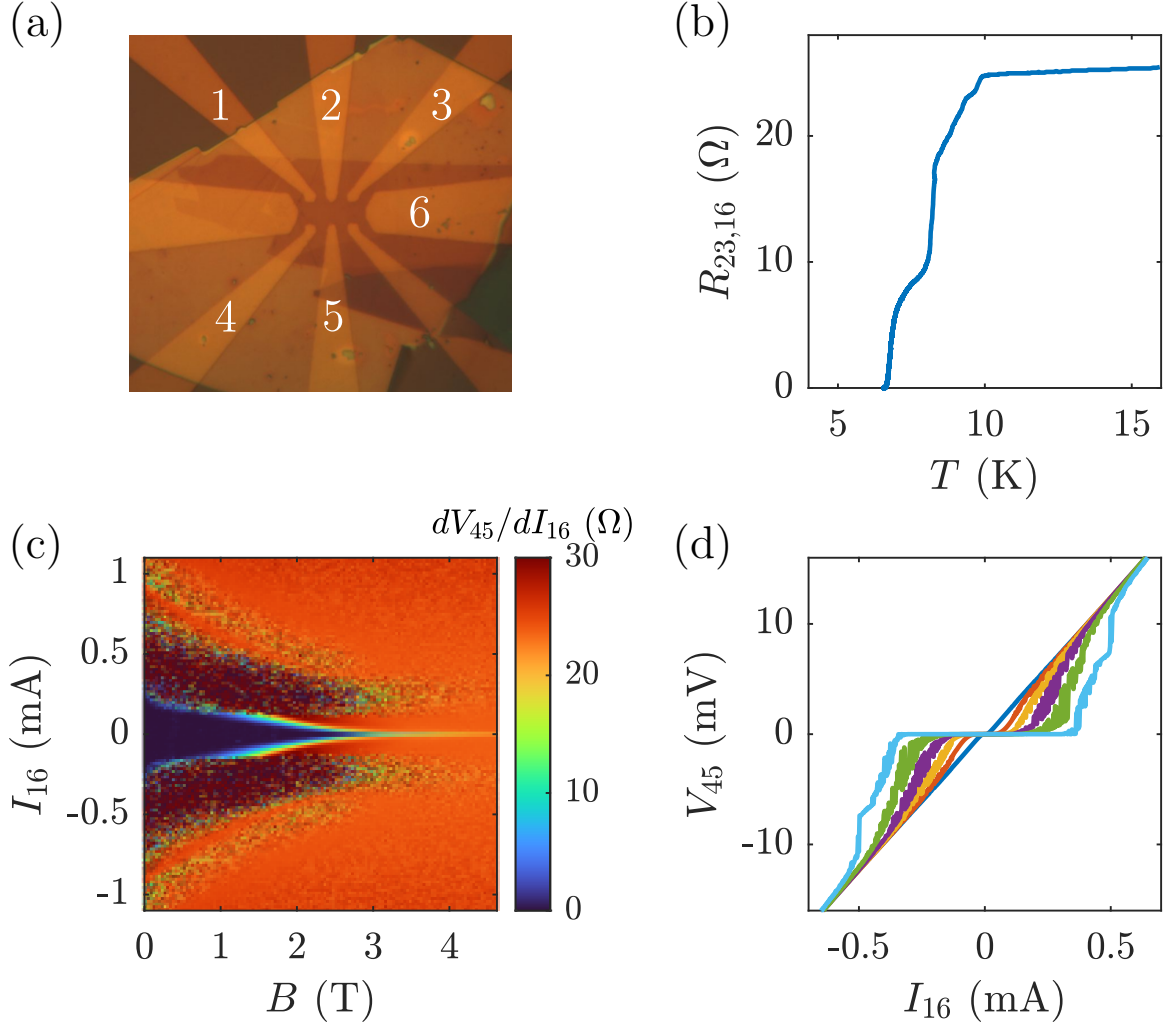


Fig. S1. (a) Optical micrograph of another thin device. Similarly to the main text, exfoliated NbSe₂ flake is put on pre-patterned gold contacts and is then covered with hBN flake. (b) Temperature dependence of the four-terminal linear-response resistance $R_{23,16} = dV_{23}/dI_{16}$. (c) Color-scale plot of the four-terminal differential resistance dV_{45}/dI_{16} as a function of the magnetic field and the bias current. (d) Current-voltage characteristics of data from panel (c) at specific values of $B = 0, 0.46, 0.97, 1.43, 1.94$ and 2.91 T.

II. THICK FLAKE

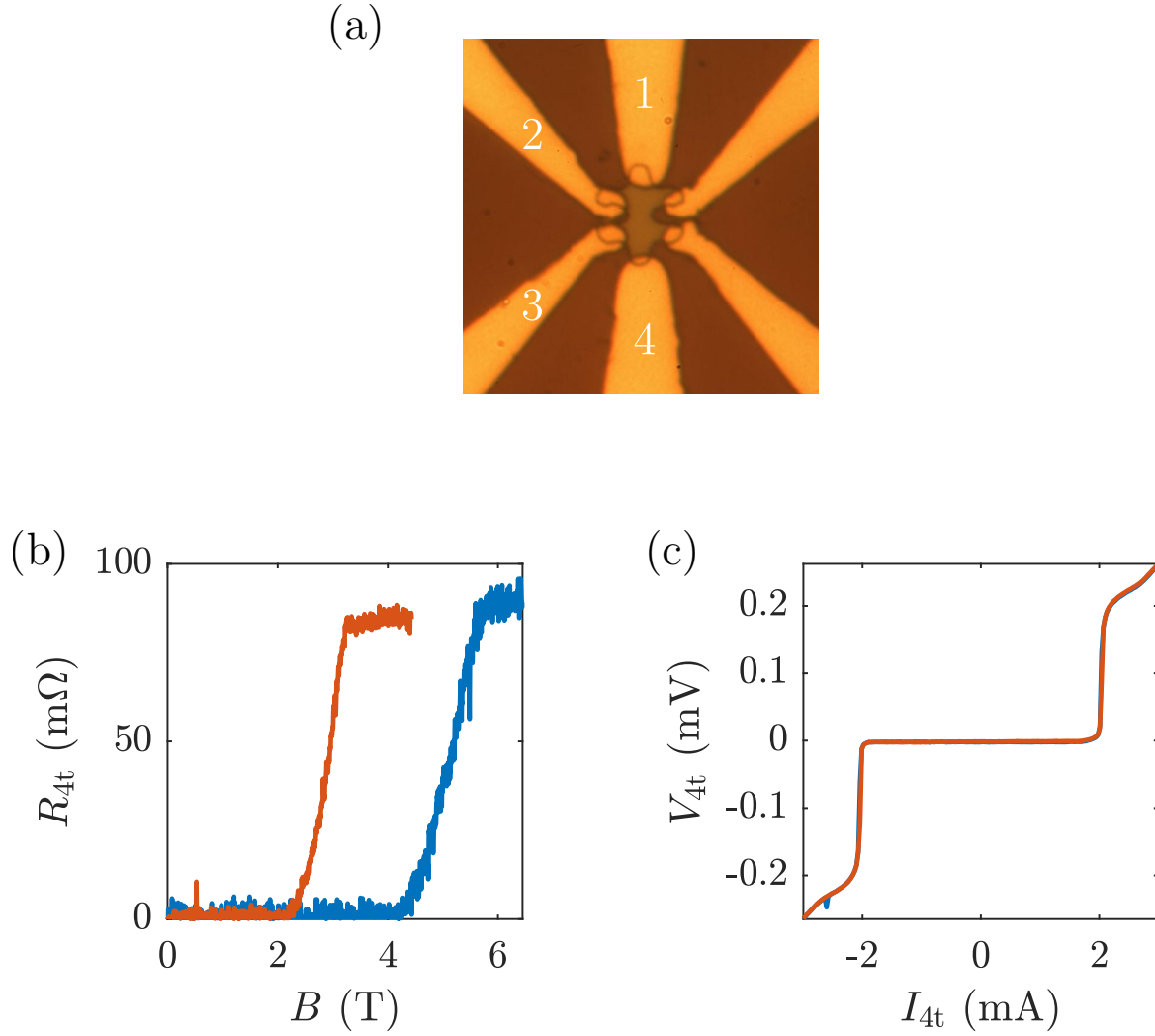


Fig. S2. (a) Optical micrograph of a relatively thick device with lithographically realized contacts. (b) Magnetic field dependence of a four-terminal resistance at $T = 4.2$ K (red curve) and $T = 0.5$ K (blue curve). (c) Four-terminal current-voltage characteristics measured at $T = 4.2$ K for two opposite current sweep directions.

III. ANOTHER TUNNEL JUNCTION ON A THIN FLAKE

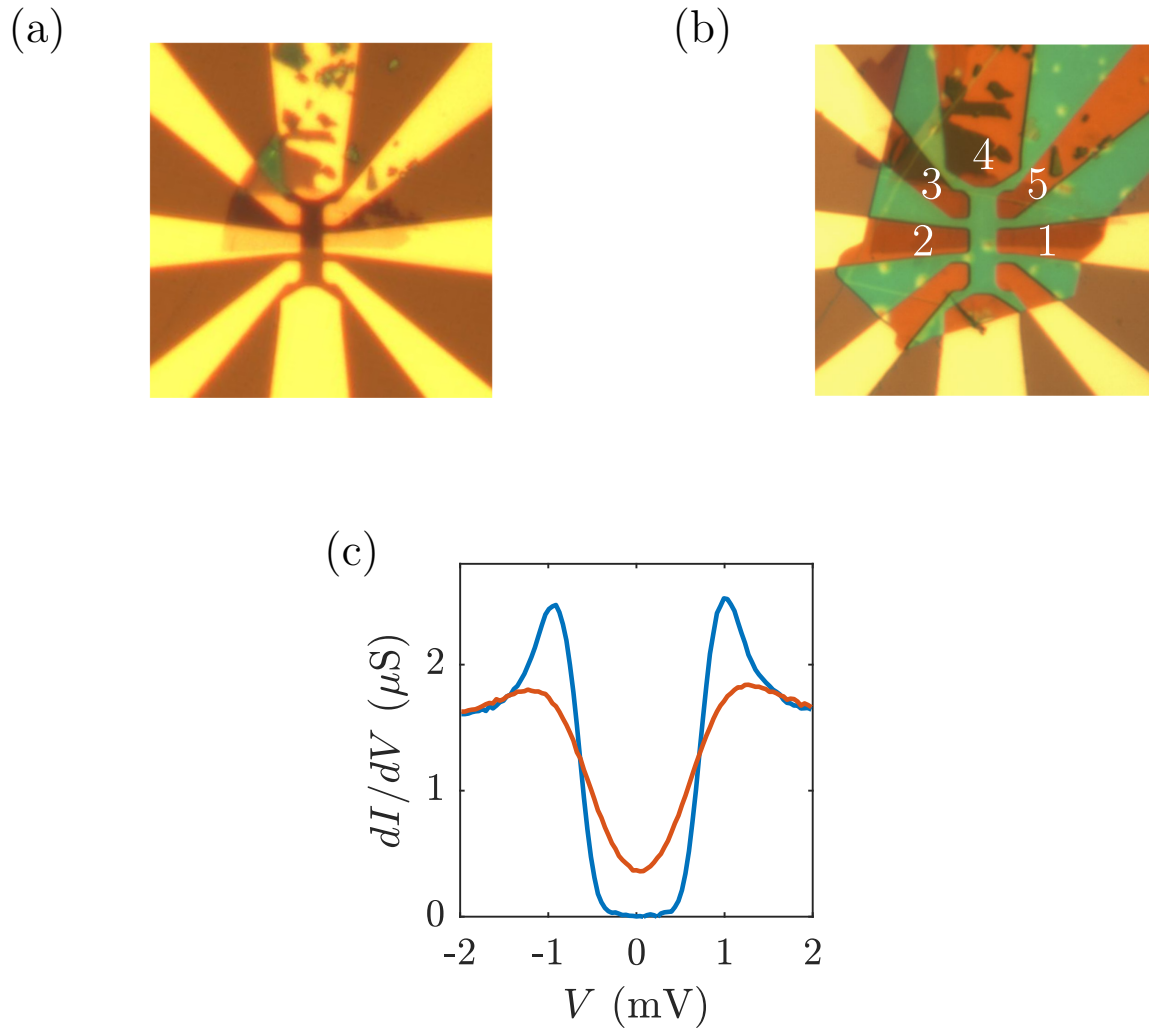


Fig. S3. (a,b) Optical micrograph of a thin device put on predefined gold contacts (a) before and (b) after coverage with hBN flake. Contacts 1, 2, 3 and 4 are in the few hundred Ohms range, contact 5 demonstrates tunnelling characteristics. (c) Differential conductance of contact 5 at $T = 3$ K (red) and $T = 0.7$ K (blue).

IV. DIFFERENTIAL RESISTANCE

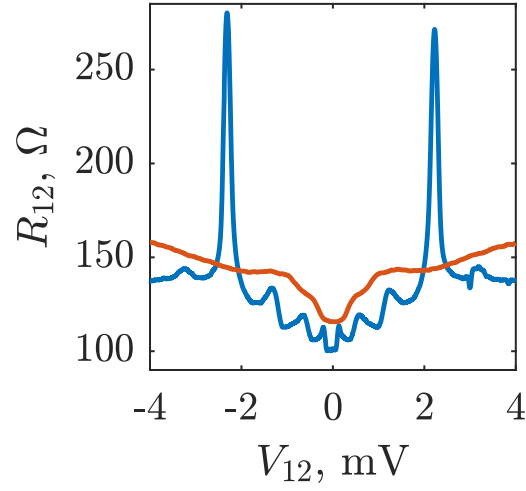


Fig. S4. Quasi- four-terminal differential resistance of the device from the main text at $T = 4.2$ K (red curve) and at $T = 0.7$ K (blue curve). The peaks are completely absent at $T = 4.2$ K.

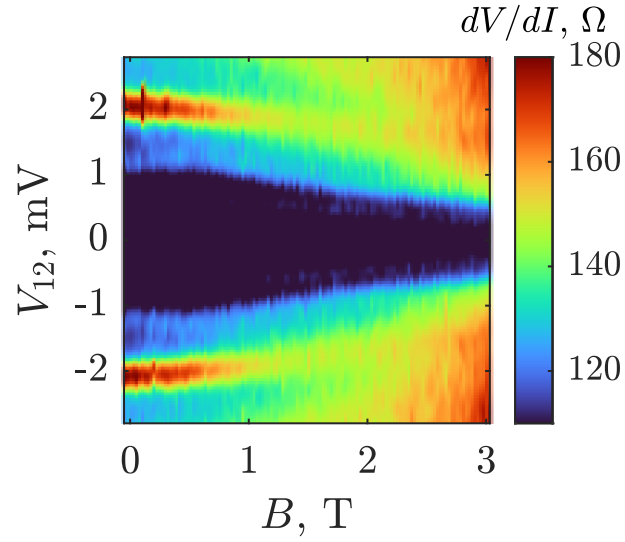


Fig. S5. Evolution of differential resistance R_{12} of the device from the main text with magnetic field and bias voltage at $T = 0.7$ K.